HHS Public Access

Author manuscript

Hear Res. Author manuscript; available in PMC 2024 June 13.

Published in final edited form as:

Hear Res. 2022 September 01; 422: 108551. doi:10.1016/j.heares.2022.108551.

Age-related stereocilia pathology in the human cochlea

Pei-zhe Wu[1,2,*], **M. Charles Liberman**[1,2]

[1]Eaton-Peabody Laboratories, Massachusetts Eye and Ear, Boston, MA 02114

[2]Department of Otolaryngology Head & Neck Surgery, Harvard Medical School, Boston, MA 02115

Abstract

Age-related hearing loss in humans is characterized by progressive loss of threshold sensitivity, especially at high frequencies. A multivariable regression of histopathological metrics from normal-aging human cochleae (Wu et al., 2020) showed that hair cell loss better predicts the audiometric shifts than either neural loss or strial atrophy, however considerable variability in age-related threshold elevation remained unexplained. Here, we develop and apply an algorithm to quantify stereocilia pathology in high-power confocal images of inner and outer hair cells in normal aging human cochleae, aged 21 – 71 yrs. Microdissected epithelial wholemounts of the cochleae were immunostained for myosin VIIa and espin to show cuticular plates and stereocilia, respectively, and each cochlea was imaged at 10 log-spaced locations along the cochlear spiral. An approach based on Fourier transforms was used to quantify the regularity of each stereocilia bundle, and the outcome was compared to a parallel analysis by a human observer. Results show a significant age-related decline in stereocilia regularity and increase in stereocilia loss and fusion. Stereocilia pathology was especially severe on the outer hair cells and in the basal half of the cochlea, and may represent a key contributor to age-related threshold elevations. For the one case with an associated pre-mortem audiogram, the threshold shifts are better predicted from the pattern of stereocilia damage than from the pattern of hair cell loss alone.

[*]Corresponding author: Pei-zhe Wu, M.D., Ph.D., Eaton-Peabody Laboratories, Massachusetts Eye and Ear Infirmary, 243 Charles St., Boston, MA 02114-3096, USA. Peizhe_Wu@meei.harvard.edu.

Author Contributions

PZW and MCL both contributed to all aspects of the study, from conception, to data acquisition, analysis and manuscript preparation.

Author statement

We are submitting a revised version of our manuscript describing a quantitative analysis of stereocilia in the human cochlea for publication in Hearing research, Major revision submitted in Feb,2022 as ‘HEARES-D-21–00351’. The editorial advice was ‘Minor Revision’.

We believe that this revised manuscript addresses all the issues raised by you and reviewers. We have changed the title, modified the method, rewritten sections of the text.

We believe our work will be of interest to readers of this Journal as it sheds important new light on the search for cause of human presbycusis and provides new insight into the functionally important structures of the inner ear.

Code Availability Statement

The Code that support the findings of this study are available from the corresponding author upon reasonable request.

Competing Interests Statement

The authors have no conflicts of interest or relevant financial relationships to disclose

Introduction

Cross-sectional studies of human hearing show progressive loss of threshold sensitivity with increasing age, especially for high-frequency tones (Pearson et al., 1995; Robinson and Sutton, 1979). This age-related hearing loss, also known as presbycusis, arises primarily in the inner ear where sound-induced mechanical vibrations are normally transduced into electrical signals in the auditory nerve. Since the inner ear cannot be imaged *in vivo* with cellular-level resolution, insights into the tissue damage underlying presbycusis can only be gained through histopathological analysis of autopsy material (Merchant and Nadol, 2010). Recent light-microscopic study of human inner-ear tissues suggested that age-related threshold shifts are best predicted by the fractional loss of outer and inner hair cells (Wu et al., 2020). However, the discrepancies between measured and predicted hearing levels suggested there might be age-related changes in hair cell condition not captured by assessing cell survival alone.

In animal studies of noise-induced hearing loss, stereocilia damage on surviving hair cells can account for much of the permanent threshold shifts observed, even years after noise exposure (Engstrom, 1983; Engstrom and Borg, 1983; Liberman and Dodds, 1984; Mulroy, 1982). This is reasonable from a functional perspective, since the mechanoelectric transduction channels fundamental to hearing are located at the tips of the stereocilia (Assad et al., 1991; Hudspeth, 1982; Pickles et al., 1984). The histopathology literature on age-related hearing loss has also documented the presence of stereocilia pathology in both animal models and human specimens, mostly based on scanning electron microscopy (Bullen et al., 2020; Engstrom et al., 1983; Nomura and Kawabata, 1979; Wright, 1983). The pathology observed in aging ears includes disarray and loss of stereocilia, as well as fusion of adjacent stereocilia membranes and marked elongation of the stereocilia bundles. However, the existing documentation of this age-related stereocilia pathology consists solely of “representative images” and summary descriptions. There are no published studies of presbycusis that quantify stereocilia pathology systematically as a function of cochlear location, to allow a rigorous evaluation of the extent to which such pathology contributes to the threshold elevations of presbycusis. From a clinical perspective, a thorough understanding of the role of stereocilia pathology in human hearing loss is important, because a therapy to regenerate stereocilia might be easier to develop than one to elicit hair cell regeneration *de novo* (Yang et al., 2012).

Here, we set out to develop a rapid and objective method to quantify stereocilia pathology in human inner ear specimens from high-resolution confocal images of the sensory epithelium. We use light microscopy rather than scanning electron microscopy to allow simultaneous and systematic analysis of surface structures, such as stereocilia, and embedded structures, such as synaptic puncta. We visualized the hair cells with myosin immunostaining and the stereocilia by using antibodies for espin, an actin cross-linking protein abundantly expressed in sensory hairs in all mammalian hair cells (Sekerkova et al., 2006). We used Fourier transforms to quantify the regularity of the hair bundle and compared these computer-driven metrics to a semi-quantitative analysis of the stereocilia pathology by a human observer from randomized single-bundle thumbnail images. The data suggest that stereocilia regularity decreases and stereocilia loss increases with increasing age, especially

on the outer hair cells in the basal half of the cochlea, thereby providing a promising explanation for much of the otherwise unexplained threshold shift of human presbycusis.

Methods

Case selection and cochlear processing

The materials for the study are human temporal bones obtained at autopsy. Except for one case, the 51 yr old, who had received a single dose of Cisplatin three months before death, all other cases in this study had no overt otologic disease and no exposure to known ototoxic agents based on medical histories and autopsy reports. Cases ranged in age from 21 to 71 yrs. Post-mortem times for the five ears were 10 hrs (21 yrs), 12 hrs (31 yrs), 7 hrs (51 yrs), 5.6 hrs (61 yrs), and 8 hrs (71 yrs). Ears were extracted with a bone-plugging tool (Merchant and Nadol, 2010; Schuknecht, 1974) soon after death and immediately immersed in buffered 10% formalin after opening the round and oval windows. After post-fixation for at least 6 days, the bone plug containing the cochlea was drilled to remove as much of the petrous bone as possible, and then immersed in EDTA at room temperature for roughly 4 weeks. The decalcified cochlea was then microdissected into 8–9 pieces, each containing the osseous spiral lamina and the attached organ of Corti. Following immunostaining, the cochlear spiral was mapped by tracing an arc along the tunnel of Corti, and normalized cochlear length was converted to frequency using a type of Greenwood function (Greenwood, 1990) modified to produce best frequencies at the very apex and base of the cochlea of 100 Hz and 20 kHz respectively. Ten frequency locations from 0.5 to 16 kHz were calculated at half-octave intervals along the length of the spiral and displayed on low-power images of the microdissected pieces to pinpoint the image-acquisition loci in each case.

Immunostaining protocols

Microdissected cochlear pieces underwent a freeze/thaw step in 30% sucrose to permeabilize them, followed by 1 h at room temperature in a blocking buffer (PBS with 5% normal horse serum and 0.3–1% Triton X-100). Tissue was then incubated overnight at 37°C with some combination of the following primary antibodies in PBS with 1% normal horse serum and 0.3–1% TritonX: (1) rabbit anti-Myosin VI and/or VIIa (Proteus Biosciences #25–6791 and 25–6790, respectively) at 1:100 to count hair cells and (2) Espin (Sigma #HPA028674) at 1:100 to identify stereocilia. Primary incubations were followed by two sequential 60-min incubations at 37°C in species-appropriate secondary antibodies (coupled to Alexafluor dyes) in PBS with 1% normal horse serum and 0.3–1% TritonX. After immunostaining, all pieces from each cochlea were slide-mounted in Vectashield, coverslipped, and the coverslip was sealed with nail polish.

Image acquisition and hair cell fractional survival analysis

For stereocilia analysis, confocal z stacks were acquired with 0.27 to 0.32 μm z-spacing on a Leica SP8 using a 63x glycerol objective (1.3 N.A.), at 10 equally spaced locations along the spiral each spanning 120 μm (roughly 13 IHCs and 39 OHCs) and comprising 2664 × 2664 pixels in x and y (16-bit depth per channel). Oversaturation of the image was avoided during acquisition: maximum saturation across all the images in this study is 60%. At each location,

the hair bundles were imaged from cuticular plate to stereocilia tips. The image was then deconvolved using the "Lightning" package on the Leica SP8, and the espin channel was then exported to a custom Matlab program for further analysis. For quantifying hair cell survival, a separate z-stack (0.33 μm z-spacing) was acquired at each location with a lower digital zoom, spanning an area roughly twice as big (246 × 246 μm).

Stereocilia analysis

At each frequency location, the z-stack was cropped into cubes, each containing one hair cell. The x,y boundary of the cube was determined by manually placing a rectangular box (10μm x 10μm) on the maximum projection of the z-stack in a custom Matlab interface. All the hair cells in each acquired stack were used in the subsequent analysis, except those truncated at the edge of the z-stack or those with no stereocilia (i.e. no signal in espin channel). The number of hair cells analyzed in this study is shown in Supplementary Figure 1.

For each hair bundle, the regularity was assessed in two ways: 1) by an observer applying a semi-quantitative rating to each image in a randomized montage of single-bundle thumbnails, and 2) by an objective regularity index based on a Fast Fourier Transform of each cropped bundle. See Results for further details.

Results

Overview of hair cell loss and audiometric data

The present study is based on analysis of five human temporal bones, representing all our recently acquired cases with post-mortem times ≤ 12 hrs, for which a stereocilia marker (espin) was included in the four-color immunolabeling protocol. These five cases ranged in age from 21 to 71 yrs, and differed little in the degree of IHC loss within cochlear regions tuned to audiometric frequencies 0.25 – 8.0 kHz (Fig. 1A). The hair cell counts in all cases except the youngest (21 yr old) show the loss of IHCs and OHCs in the extreme base that is classic for age-related hearing loss (Bredberg, 1968; Schuknecht, 1955). The marked OHC loss in the apical cochlea, especially in the 61 yr old, has recently been shown to be quite common in aging humans (Wu et al., 2020; Wu et al., 2019).

Audiometric data were available only for the oldest ear (Fig. 1C). The high-tone hearing loss in this case represents the classic pattern for presbycusis; however, aligning the audiogram to the pattern of hair cell loss suggests that the precipitous loss of hearing sensitivity above 2 kHz is not well explained by the pattern of hair cell loss alone. The OHC loss in the extreme apex is not reflected in the audiogram, because it appears at cochlear frequencies below those routinely tested.

Qualitative assessment of stereocilia condition

The presence of threshold elevation, in this case, in regions of minimal hair cell loss between 2 and 8 kHz is not surprising considering that surviving sensory cells may not be fully functional. Given the well-documented role of stereocilia damage as a major contributor to noise-induced permanent threshold shifts in animal models (Liberman and Dodds, 1984),

we sought to evaluate stereocilia condition in our freshly acquired human material. We incorporated antibodies against espin, an actin cross linker richly expressed in the stereocilia bundle (Sekerkova et al., 2006), into the immunoprocessing of our whole-mount dissections of human temporal bones.

Confocal images from these specimens revealed all the major types of stereocilia pathology described in scanning electron micrographs from aging human and animal cochleae, i.e. disarray, fusion, loss, and elongation of stereocilia (Figs. 2 and 3). Stereocilia elongation was present in all but the youngest ear, but only at the extreme apex, i.e. cochlear frequency regions at and apical to the 0.25 kHz place. As shown in Figure 2, that elongation could be spectacular, even in a 31 yr old.

Among the other stereocilia abnormalities, disarray can be a stand-alone pathology while the other pathologies often co-exist on the same cell, e.g., on a hair cell with stereocilia loss, the remaining stereocilia are often fused and/or disarrayed, and fused stereocilia are often elongated. The striking differences in the prevalence of these stereocilia pathologies between a younger (21 yrs) and an older cochlea (71 yrs) are obvious in Figure 3, which shows a maximum projection view of the IHCs and first two rows of OHCs at the 5.6 kHz region.

Among IHCs in Figure 3, the 21 yr old shows significant bundle disarray: sometimes the bundle is bent away from the OHCs such that the taller row obscures the shorter rows (e.g. on cells 8 and 9 in Fig. 3 top panel), while, on other cells, parts or all of the bundle are bent towards the OHCs (cells 10 and 6 in Fig. 3 top panel, respectively). However, among the 21 yr old's IHCs, there is virtually no loss or fusion of stereocilia, and, on each bundle, 15–20 individual tall-row stereocilia can be discerned. Contrast this with the IHCs in the image from the 71 yr old (Fig. 3). Discrete stereocilia of the same caliber as those in the young bundles are extremely rare, and at least two of the cells show prominent fusion bundles (white arrowheads). A surprising number of cells show no espin staining at all (red arrowheads), although in some cases, the Myosin7a stain suggests that there are remaining microvillous extensions (i.e. stereocilia) that no longer contain espin crosslinking (green arrowhead). Note that the myosin staining tends to be weaker in those IHCs and OHCs lacking espin expression, suggesting that the affected cells are generally less healthy.

In the OHC area of the 21 yr old, two sensory cells are missing (white X's in Fig. 3), however, none of the hair bundles on surviving cells shows any obvious loss or fusion, and even the disarray is minimal. In contrast, in the older specimen, in addition to hair cell loss, many of the surviving hair bundles show gaps in the stereocilia array (blue arrowheads) or fusion bundles (white arrowheads). As with the IHCs, numerous OHCs in the older ears show no espin label (red arrowheads).

Semi-quantitative assessment of stereocilia condition

To evaluate these age-related trends more systematically, we cropped the maximum projection images from all five cases at all 10 cochlear regions into an array of single-bundle thumbnails. We randomized the thumbnails and asked a blinded observer to apply a four-level rating scale based on the degree of stereocilia fusion (Fig. 4). We chose to ignore stereocilia disarray, because it is ubiquitous in scanning electron microscopy of control ears

(Rhodes et al., 2004; Soucek et al., 1987), and is logically an unavoidable result of the mechanical handling involved in tissue preparation. The scaling criteria were as follows: “3” if < 30% of stereocilia are fused; “2” if > 30% of stereocilia are fused BUT > 50% are still < 3X normal width; “1” if > 30% of stereocilia are fused AND > 50% of stereocilia are > 3X normal width; and “0” if there was no stereocilia bundle remaining on a surviving cell.

Exemplar thumbnails for both OHCs and IHCs are shown in Figure 4, with one example of each rating at each cochlear region within the audiometric frequency range. The appearance of the “normal” OHC bundles (rating “3”) changes systematically from apex to base as the height of the stereocilia decreases. In this coverslipped material, the longer stereocilia tend to bend at their points of hair cell insertion such that only the tallest row is visible. In the high-frequency region, where the OHC stereocilia are shorter, and stiffer (Strelioff and Flock, 1984), the bundles remain more erect and the hexagonal patterning of the multiple stereocilia rows is often revealed in the normal bundles. In the pathological OHC bundles, the fusion is sometimes restricted to clusters of 2 or 3 adjacent stereocilia, which gives rise to the “2” rating, and other times involves greater numbers of adjacent elements, giving rise to a “1” rating. The viewing orientation of the IHC bundles remains more constant throughout the cochlea, and their length appears to change less with cochlear location (Kaltenbach et al., 1994).

The results of our semi-quantitative analysis (Fig. 5) show that bundle fusion was the most severe and widespread in the 71 yr old, in both the IHC and OHC areas. The least severe bundle fusion was seen in either the 31 yr old (IHCs, Fig. 5A) or the 21 yr old (OHCs, Fig. 5B), and the alignment of stereocilia condition with the audiogram in the 71 yr old (Fig. 5C) suggests that the high-tone hearing loss of this presbycusic individual might be explained by the accumulation of stereocilia fusion in the OHC area rather than by considering only the pattern of OHC death. The exceptionally low mean scores for the IHCs throughout the 71 yr old ear arise predominantly from the high number of IHCs completely lacking a stereocilia bundle, which are rated ‘0’. The prevalence of these “0” ratings is well seen in the cumulative distributions, pooled across apical and basal halves of the cochlea (Fig. 5D-F). In these plots, the y value at which the cumulative rating exceeds 0 shows the percentage of cells lacking all stereocilia, i.e. > 45% of IHCs in the 71 yr old in both the apical and basal halves of the cochlea. The maximum cumulative rating for each curve indicates the mean stereocilia rating for that sample, i.e. 1.1 for OHCs in the 71 yr old in basal half of the cochlea. Note that, in the OHC cumulative plots, the curves are well ordered by increasing pathology with increasing age.

Fourier analysis of hair bundle regularity

Given the regularity of stereocilia in a normal hair bundle, we reasoned that image analysis based on spatial frequency, i.e. Fast Fourier Transform (FFT), might provide a sensitive and objective metric of the stereocilia pathology in the hair bundles from aging ears, especially in the OHC area where stereocilia disarray from mechanical artifact appears to be less of a confound (Fig. 3).

For this analysis, we started with the same single-bundle crops of the image stacks (each 10 μm by 10 μm in X and Y) used for the semi-quantitative analysis: see Suppl Fig 1

for a summary of the number of bundles analyzed in each case at each frequency region. However, rather than using the maximum projection images, we applied 2D FFT analysis to 10 contiguous single slices from the middle of the z-stack (Fig. 6C) and then computed the maximum projection of the 2D spectra (Fig. 6D). This 2D FFT can be viewed as a spectrum in polar coordinates (Fig. 6D), with the spectral radius proportional to spatial frequency, the signal amplitude depicted as a heatmap, and the rotation angle at which the slice was scanned displayed around the circumference. Note that the spectrum has rotational-image symmetry at 180° across the equator. The 2D FFT in Figure 6D shows significant periodicity at ~ 2.9 cycles/μm (corresponding to stereocilia spacing of 0.35 μm). The rotational angle indicated by the red axes in Fig. 6D intersects a high-amplitude patch, because it aligns well with the stereocilia: the red axes in the inset to Fig. 6B are at the same rotational angle. The spectral amplitude peaks at 6 different rotational angles (Fig. 6E, three pairs of peaks with each pair spaced 180° apart), because of the periodicity inherent to the hexagonal packing pattern of the stereocilia (see the three pairs of axes in the Fig. 6B inset).

At each spatial frequency, a “regularity index” was defined, as the peak spectral amplitude across all rotation angles minus the noise floor (Fig. 6E), i.e. the peak amplitude at a low spectral frequency (Fig. 6F). In the youngest ear, the mean regularity index, averaged across all hair cells at each cochlear frequency, peaks at lower spatial frequencies for IHCs than OHCs (Fig. 6F,G). Regardless of cochlear location, the peak values for IHCs are near 1.9 cycles/μm, corresponding to a mean stereocilia spacing of 0.52 μm (Fig. 6G). This corresponds well with reported values of 0.4 – 0.5 μm for IHC stereocilia thickness in hamster, regardless of cochlear location (Kaltenbach et al., 1994). For OHCs, the stereocilia are thinner, and the regularity index peaks at higher spatial frequencies (2.5 – 3.2 cycles/μm), especially in the basal half of the cochlea where the inter-stereocilia spacing is 0.32 μm (Fig. 6F). OHC stereocilia thickness was not measured in the prior hamster study,

A normal stereocilia (rating of “3”) has a symmetrical 2D spectrum with the amplitude peaks at a constant spectral frequency (Fig. 7A). The regularity index of a massively fused bundle (rating of “1” in Fig. 7C) peaks at a lower frequency than normal and is negative at the target spatial frequency. The regularity index of a bundle with stereocilia fused to a lesser degree (rating of “2” in Fig. 7B) shows no prominent spectral peak because the inter-stereocilia spacing is less uniform, and the regularity index is near zero.

The mean regularity indices for all bundles analyzed are summarized in Figure 8. The summary data for OHCs (Fig. 8B) show similar trends to those seen in the semi-quantitative analysis (Fig. 5B): 1) the regularity is markedly lower in the three older ears than in the two younger ears, and 2) there is a general apical-basal trend towards lower regularity, especially in the older cochlea. Indeed, the correlations between the FFT-based and the observer-based scores are very good (Fig. 8D, $r^2 = 0.62$, $p < 0.001$). The summary FFT data from the IHC area show little evidence for apical-basal trends (Fig. 8A), but the correlations between the FFT and observer ratings are still significant (Fig. 8C, $r^2 = 0.23$, $p < 0.001$). Although the IHC bundles from the oldest ear received generally poor scores from the observer and the FFT analysis, many bundles getting high observer scores were found to be highly irregular by FFT. This discrepancy arises because stereocilia disarray, which the observer was instructed to ignore, is more common among the IHCs. For example, the IHC bundle at

2.0 kHz in Figure 4 was rated as “3” by the observer, because there is no fusion, but the FFT score is diminished by the bundle disarray. The full observer-based scores in Figure 5 show a more prominent age effect, because they include the “0” ratings for cell with no stereocilia, but such cells could not be analyzed via FFT.

Discussion

Prior histopathological studies have suggested that loss of hair cells, atrophy of the stria vascularis, and loss of auditory-nerve fibers are all important contributors to the steady loss of high-frequency hearing that degrades auditory function in the aging human ear (Pauler et al., 1988; Ramadan and Schuknecht, 1989; Schuknecht, 1955, 1964; Schuknecht, 1974; Schuknecht and Gacek, 1993; Schuknecht et al., 1974). Using a multivariable regression analysis on quantitative histopathological data from a large sample of aging humans, we concluded that, of these pathologies, hair cell loss in the appropriate cochlear region was the best predictor of the threshold shifts (Wu et al., 2020). However, the hair cell loss patterns only explained 65% of the variance in audiometric thresholds, and factoring in the strial atrophy and loss of auditory nerve fibers did not improve the threshold prediction, although both were commonly seen.

In animal models of permanent noise-induced hearing loss, large threshold shifts are often seen in ears in with minimal loss of sensory cells, and in which all accessory tissues of the cochlear duct, e.g. stria vascularis, limbus, spiral prominence, and spiral ligament) appear normal at the light microscopic level (Liberman and Dodds, 1984; Liberman and Kiang, 1978). In such cases, there is often widespread damage to the stereocilia (Liberman and Dodds, 1984), the microvillar tuft on the apical surface of each hair cell, where the mechanoelectric transduction channels are located. Given that the sound-evoked opening of these channels relies on delicate extracellular connections between adjacent stereocilia (Hudspeth, 1989), it is not surprising that disarray, loss or fusion of stereocilia on surviving hair cells could result in significant threshold elevation.

A number of prior studies, mostly using scanning electron microscopy (SEM), have documented the hair-bundle pathology in noise-exposed, or aging, human or animal cochleae, including disarray, loss, fusion and elongation of stereocilia on both inner and outer hair cells (Engstrom, 1984; Engstrom and Borg, 1983; Mulroy, 1982; Nomura and Kawabata, 1979; Wright, 1982). The vast majority of these studies have been on noise-exposed animals. Only a handful of these animal studies have attempted to quantify the damage in any systematic way, instead of relying on overall impressions and “representative” images. These qualitative studies agree that both noise and aging increase the frequency of stereocilia fusion (Engstrom, 1984; Engstrom and Borg, 1983; Liberman and Dodds, 1984), especially on IHCs (Engstrom, 1983; Engstrom et al., 1983), and that stereocilia elongation is more common in the apical half of the cochlea than in the base (Wright, 1982).

The quantitative approaches to stereocilia pathology assessment taken in the past have included 1) counting the number of hair cells with fused stereocilia (Engstrom and Borg, 1983), and 2) counting, for each hair bundle, on each hair cell, the number of surviving

stereocilia that remained with 30° of vertical (Liberman and Dodds, 1984). The latter study was done at the light-microscopic level on cochleae that were plastic-embedded immediately after fixation, and before any drilling or mechanical handling of the delicate pieces of sensory epithelium. These animal studies of noise-induced stereocilia pathology suggest that the extent and degree of stereocilia damage is well correlated with the frequency range and severity of the threshold shift (Engstrom, 1983, 1984; Engstrom and Borg, 1983; Liberman and Dodds, 1984, 1987).

The semi-quantitative metric we developed for the present study concentrated on fusion and loss of stereocilia, explicitly ignoring disarray, because we believe that fusion and loss are less prone to mechanical or post-mortem artifact. Even in the youngest ears, the hair bundles on IHCs and apical OHCs were often disarrayed. We speculate that this arises from the handling and/or coverslipping of wet-dissected material. The patterns of disarray in the present study are consistent with the fact that IHC bundles are less stiff than OHC bundles and that OHC bundles are less stiff in the apical cochlea than in the base by a factor of 50 (Strelioff and Flock, 1984). The apical-basal gradient in OHC bundle stiffness is likely related to the fact that there are 3X the number of OHC stereocilia per hair cell at the base, with up to 5 rows of stereocilia on each bundle, than at the apex, with only 3 rows per bundle (Wright, 1981).

There is limited information on the effect of post-mortem autolysis on stereocilia morphology. One SEM study in guinea pig compared stereocilia from 15 minutes to 4 hours post mortem and saw subtle changes in the smoothness of the stereocilia membranes (Osborne et al., 1989), which would not be visible at the level of resolution of our confocal images. There was no evidence of postmortem artifact related to the fusion, loss or disarray that we are capturing here with our algorithm. Another animal study evaluated the effects of hypoxia on cochlear morphology (Shirane and Harrison, 1987) and noted “blebbing” of the apical surface, where a membrane blister forms by extrusion of cytoplasm through the hole in the actin matrix of the cuticular plate where the kinocilium was located during development (Liberman, 1987). We never saw such cytoplasmic blisters, but it is possible that they do not contain myosin 7a or espin and are thus invisible in our confocal images. In a human study, comparing the morphology of ears fixed at increasing times after death, the authors noted dramatic vacuolization and swelling of neural terminals at the neural pole of the hair cells but make no mention of increasing prevalence of fusion, or loss of the stereocilia tufts as post-mortem time increases (Nadol and Burgess, 1985). Here, the fact that the 21 yr old, with the most regular stereocilia, also has the longest post-mortem time argues against this issue as a major confound in the present study.

The time-consuming nature of observer-driven stereocilia analysis led us to develop a computer-driven algorithm, and an FFT analysis of spatial periodicity has proven to be a fruitful approach. Algorithms using spatial autocorrelation have been used in the past to quantify the arrangement of stereocilia in normal bundles on vestibular hair cells (Rowe and Peterson, 2004). Such algorithms rely on the stereotypical hexagonal lattice, which, in our cochlear material, is most clearly visible for OHC bundles in the basal half of the cochlea. Fortuitously, basal-turn OHCs are also likely a major locus of pathology in the aging ear. Our FFT metric is influenced by any pathology that disrupts the normal

periodicity of the bundle, including fusion, loss or disarray of stereocilia. Disarray may be artifactual in cochleae that are “wet-dissected”, as employed here for confocal microscopy or in other studies for scanning electron microscopy. Although this mechanical artifact can be minimized by embedding the cochleae in plastic before the microdissection step (Bohne, 1972; Liberman and Dodds, 1984) and viewing the organ of Corti with high-N.A. immersion objectives directly through the polymerized plastic (Liberman and Dodds, 1984), plastic embedding doesn’t allow fluorescent immunostaining or confocal imaging.

The FFT algorithm developed here can also be applied to cochleae from experimental animals, especially larger experimental animals such as guinea pigs and gerbils, where cochlear function can be routinely obtained, and tissue fixation can be better controlled. Implementing the algorithm in mice is challenging because the stereocilia are small in caliber and the spacing between them falls below the resolution of conventional confocal microscopy, which greatly reduces the periodicity signal. Use of imaging techniques with higher resolution, such as structured illumination (Ebrahim et al., 2016), can produce stereocilia images even in mice that are amenable to Fourier analysis.

As we slowly accrue more human specimens, especially those with audiograms taken close to death, both the objective and subjective algorithms can be used to rigorously test the contribution of stereocilia pathology on surviving hair cells to the accumulating threshold shifts seen in the aging ear. The limited data shown here suggest that this type of pathology could be a major aspect of the functionally important pathologies underlying presbycusis. It is not hard to imagine that the degradation of stereocilia condition we observed in the 71 yr old (Fig. 5C) fully accounts for the 60 dB threshold elevation seen in the corresponding frequency region of the audiogram in that subject (Fig. 5C). If true, the emerging therapies for sensorineural hearing loss based on transdifferentiating surviving supporting cells to replace missing hair cells (Mizutari et al., 2013) may be misdirected for many cases of presbycusis. A better targeted approach might be directed at eliciting stereocilia regeneration on surviving hair cells, as has been reported in animal models (Yang et al., 2012).

Supplementary Material

Refer to Web version on PubMed Central for supplementary material.

Acknowledgements

Research supported by a grant from the National Institute on Deafness and other Communicative Disorders (P50 DC 015857). Advice on image analysis from Drs. Denny Freeman, John Guinan and Sunil Puria is gratefully acknowledged, as is expert histological preparation and blinded stereocilia analysis by Leslie Liberman, and temporal bone procurement by Diane Jones.

Data Availability Statement

The data that support the findings of this study are available in Matlab format from the corresponding author upon reasonable request.

References Cited

Assad JA, Shepherd GM, Corey DP, 1991. Tip-link integrity and mechanical transduction in vertebrate hair cells. Neuron 7(6), 985–994. 10.1016/0896-6273(91)90343-x. [PubMed: 1764247]

Barr-Gillespie PG, 2015. Assembly of hair bundles, an amazing problem for cell biology. Mol Biol Cell 26(15), 2727–2732. 10.1091/mbc.E14-04-0940. [PubMed: 26229154]

Bohne BA, 1972. Location of small cochlear lesions by phase contrast microscopy prior to thin sectioning. The Laryngoscope LXXXII(1), 1–16. [PubMed: 4550422]

Bredberg G, 1968. Cellular pattern and nerve supply of the human organ of Corti. Acta Otolaryngol, Suppl 236:231+.

Bullen A, Forge A, Wright A, Richardson GP, Goodyear RJ, Taylor R, 2020. Ultrastructural defects in stereocilia and tectorial membrane in aging mouse and human cochleae. J Neurosci Res 98(9), 17451763. 10.1002/jnr.24556.

Engstrom B, 1983. Stereocilia of sensory cells in normal and hearing impaired ears. A morphological, physiological and behavioural study. Scand Audiol Suppl 19, 1–34.

Engstrom B, 1984. Fusion of stereocilia on inner hair cells in man and in the rabbit, rat and guinea pig. Scand Audiol 13(2), 87–92. 10.3109/01050398409043045. [PubMed: 6463557]

Engstrom B, Borg E, 1983. Cochlear morphology in relation to loss of behavioural, electrophysiological, and middle ear reflex thresholds after exposure to noise. Acta Otolaryngol Suppl 402, 5–23. 10.3109/00016488309122873. [PubMed: 6582763]

Engstrom B, Flock A, Borg E, 1983. Ultrastructural studies of stereocilia in noise-exposed rabbits. Hear Res 12(2), 251–264. 10.1016/0378-5955(83)90110-7. [PubMed: 6643294]

Greenwood DD, 1990. A cochlear frequency-position function for several species−−29 years later. J Acoust Soc Am 87(6), 2592–2605. [PubMed: 2373794]

Hudspeth AJ, 1982. Extracellular current flow and the site of transduction by vertebrate hair cells. J Neurosci 2(1), 1–10. [PubMed: 6275046]

Hudspeth AJ, 1989. How the ear's works work. Nature 341(6241), 397–404. 10.1038/341397a0. [PubMed: 2677742]

Liberman MC, 1987. Chronic ultrastructural changes in acoustic trauma: serial-section reconstruction of stereocilia and cuticular plates. Hear Res 26(1), 65–88. 10.1016/0378-5955(87)900360. [PubMed: 3558144]

Liberman MC, Dodds LW, 1984. Single-neuron labeling and chronic cochlear pathology. III. Stereocilia damage and alterations of threshold tuning curves. Hear Res 16(1), 55–74. 10.1016/0378-5955(84)90025-x. [PubMed: 6511673]

Liberman MC, Dodds LW, 1987. Acute ultrastructural changes in acoustic trauma: serial-section reconstruction of stereocilia and cuticular plates. Hear Res 26(1), 45–64. 10.1016/03785955(87)90035-9. [PubMed: 3558143]

Liberman MC, Kiang NY, 1978. Acoustic trauma in cats. Cochlear pathology and auditory-nerve activity. Acta Otolaryngol Suppl 358, 1–63. [PubMed: 281107]

Manor U, Kachar B, 2008. Dynamic length regulation of sensory stereocilia. Semin Cell Dev Biol 19(6), 502–510. 10.1016/j.semcdb.2008.07.006. [PubMed: 18692583]

Merchant SN, Nadol JB, 2010. Schuknecht's Pathology of the Ear, 3rd Edition. People's Medical Publishing House - USA, Shelton, CT.

Mizutari K, Fujioka M, Hosoya M, Bramhall N, Okano HJ, Okano H, Edge AS, 2013. Notch inhibition induces cochlear hair cell regeneration and recovery of hearing after acoustic trauma. Neuron 77(1), 58–69. 10.1016/j.neuron.2012.10.032. [PubMed: 23312516]

Mulroy MCLMJ, 1982. Acute and chronic effects of Acoustic trauma: cochlear pathology and auditory nerve pathophysiology. New Perspectives on Noise-Induced hearing loss.

Nadol JB Jr., Burgess B, 1985. A study of postmortem autolysis in the human organ of Corti. J Comp Neurol 237(3), 333–342. 10.1002/cne.902370305. [PubMed: 3900149]

Nomura Y, Kawabata I, 1979. Loss of stereocilia in the human organ of Corti. Arch Otorhinolaryngol 222(3), 181–185. 10.1007/BF00456314. [PubMed: 444152]

Osborne MP, Comis SD, Johnson AP, Jeffries DR, 1989. Post-mortem changes in hair bundles of the guinea pig and human cochlea studied by high-resolution scanning microscopy. Acta Otolaryngol 108(3–4), 217–226. 10.3109/00016488909125521. [PubMed: 2816336]

Pauler M, Schuknecht HF, White JA, 1988. Atrophy of the stria vascularis as a cause of sensorineural hearing loss. Laryngoscope 98(7), 754–759. 10.1288/00005537-198807000-00014. [PubMed: 3386381]

Pearson JD, Morrell CH, Gordon-Salant S, Brant LJ, Metter EJ, Klein LL, Fozard JL, 1995. Gender differences in a longitudinal study of age-associated hearing loss. J Acoust Soc Am 97(2), 11961205. 10.1121/1.412231.

Pickles JO, Comis SD, Osborne MP, 1984. Cross-links between stereocilia in the guinea pig organ of Corti, and their possible relation to sensory transduction. Hear Res 15(2), 103–112. 10.1016/0378-5955(84)90041-8. [PubMed: 6436216]

Ramadan HH, Schuknecht HF, 1989. Is there a conductive type of presbycusis? Otolaryngol Head Neck Surg 100(1), 30–34. 10.1177/019459988910000105. [PubMed: 2493614]

Rhodes CR, Hertzano R, Fuchs H, Bell RE, de Angelis MH, Steel KP, Avraham KB, 2004. A Myo7a mutation cosegregates with stereocilia defects and low-frequency hearing impairment. Mamm Genome 15(9), 686–697. 10.1007/s00335-004-2344-x. [PubMed: 15389316]

Robinson DW, Sutton GJ, 1979. Age effect in hearing - a comparative analysis of published threshold data. Audiology 18(4), 320–334. [PubMed: 475664]

Rowe MH, Peterson EH, 2004. Quantitative analysis of stereociliary arrays on vestibular hair cells. Hear Res 190(1–2), 10–24. 10.1016/S0378-5955(03)00395-2. [PubMed: 15051126]

Schuknecht HF, 1955. Presbycusis. Laryngoscope 65(6), 402–419. 10.1288/00005537195506000-00002. [PubMed: 14392966]

Schuknecht HF, 1964. Further Observations on the Pathology of Presbycusis. Arch Otolaryngol 80, 369382. 10.1001/archotol.1964.00750040381003.

Schuknecht HF, 1974. Pathology of the Ear. Harvard Universtiy Press, Cambrideg, MA.

Schuknecht HF, Gacek MR, 1993. Cochlear pathology in presbycusis. Ann Otol Rhinol Laryngol 102(1 Pt 2), 1–16. 10.1177/00034894931020S101.

Schuknecht HF, Watanuki K, Takahashi T, Belal AA Jr., Kimura RS, Jones DD, Ota CY, 1974.Atrophy of the stria vascularis, a common cause for hearing loss. Laryngoscope 84(10), 1777–1821. 10.1288/00005537-197410000-00012. [PubMed: 4138750]

Sekerkova G, Zheng L, Loomis PA, Mugnaini E, Bartles JR, 2006. Espins and the actin cytoskeleton of hair cell stereocilia and sensory cell microvilli. Cell Mol Life Sci 63(19–20), 2329–2341. 10.1007/s00018-006-6148-x. [PubMed: 16909209]

Shirane M, Harrison RV, 1987. The effects of hypoxia on sensory cells of the cochlea in chinchilla. Scanning Microsc 1(3), 1175–1183. [PubMed: 3659860]

Soucek S, Michaels L, Frohlich A, 1987. Pathological changes in the organ of Corti in presbyacusis as revealed by microslicing and staining. Acta Otolaryngol Suppl 436, 93–102.10.3109/00016488709124981. [PubMed: 2445165]

Strelioff D, Flock A, 1984. Stiffness of sensory-cell hair bundles in the isolated guinea pig cochlea. Hear Res 15(1), 19–28. 10.1016/0378-5955(84)90221-1. [PubMed: 6480520]

Wright A, 1981. Scanning electron microscopy of the human cochlea--the organ of Corti. Arch Otorhinolaryngol 230(1), 11–19. 10.1007/BF00665375. [PubMed: 7213191]

Wright A, 1982. Giant cilia in the human organ of Corti. Clin Otolaryngol Allied Sci 7(3), 193–199. 10.1111/j.1365-2273.1982.tb01582.x. [PubMed: 7105451]

Wright A, 1983. Scanning electron microscopy of the human organ of Corti. J R Soc Med 76(4), 269–278. [PubMed: 6341584]

Wu PZ, O'Malley JT, de Gruttola V, Liberman MC, 2020. Age-Related Hearing Loss Is Dominated by Damage to Inner Ear Sensory Cells, Not the Cellular Battery That Powers Them. J Neurosci 40(33), 6357–6366. 10.1523/JNEUROSCI.0937-20.2020. [PubMed: 32690619]

Wu PZ, Wen WP, O'Malley JT, Liberman MC, 2019. Assessing fractional hair cell survival in archival human temporal bones. Laryngoscope. 10.1002/lary.27991.

Yang SM, Chen W, Guo WW, Jia S, Sun JH, Liu HZ, Young WY, He DZ, 2012. Regeneration of stereocilia of hair cells by forced Atoh1 expression in the adult mammalian cochlea. PLoS One 7(9), e46355. 10.1371/journal.pone.0046355.

Highlights

- Stereocilia damage in hair cells can be visualized with confocal images
- The degree of stereocilia disarray, fusion and loss can be quantified algorithmically
- Stereocilia regularity decline with age, especially at higher frequencies
- Stereocilia volume decreases with age throughout the cochlea

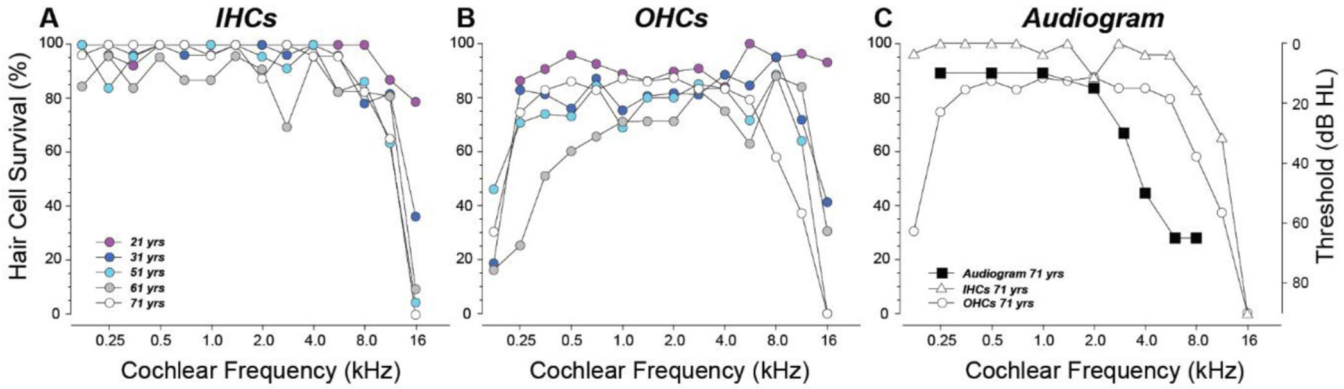

Figure 1:

Hair cell survival from each of the five specimens in this study (**A,B**) compared to the audiogram in the case where one was available (**C**). **A,B**: OHC values are the average of all rows. Symbol key in **A** also applies to **B**. **C**: Hair cell survival for the 71 yr old is replotted (from Panels **A,B**) and superimposed on the audiogram, obtained 3 yrs before death.

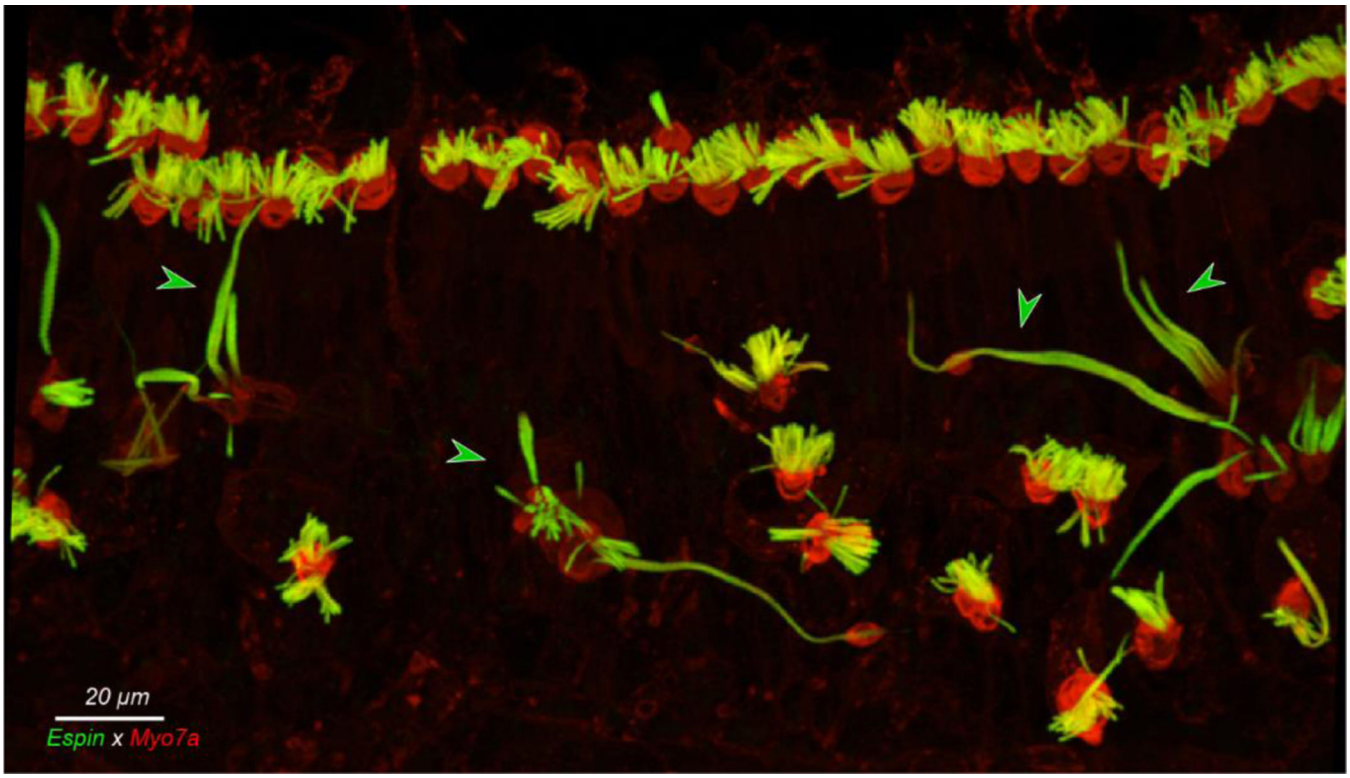

Figure 2:
Giant stereocilia are common at the extreme apex. This is the maximum projection of a confocal z-stack from the 0.175 kHz region of the 31 yr old case. Green arrowheads point to giant stereocilia.

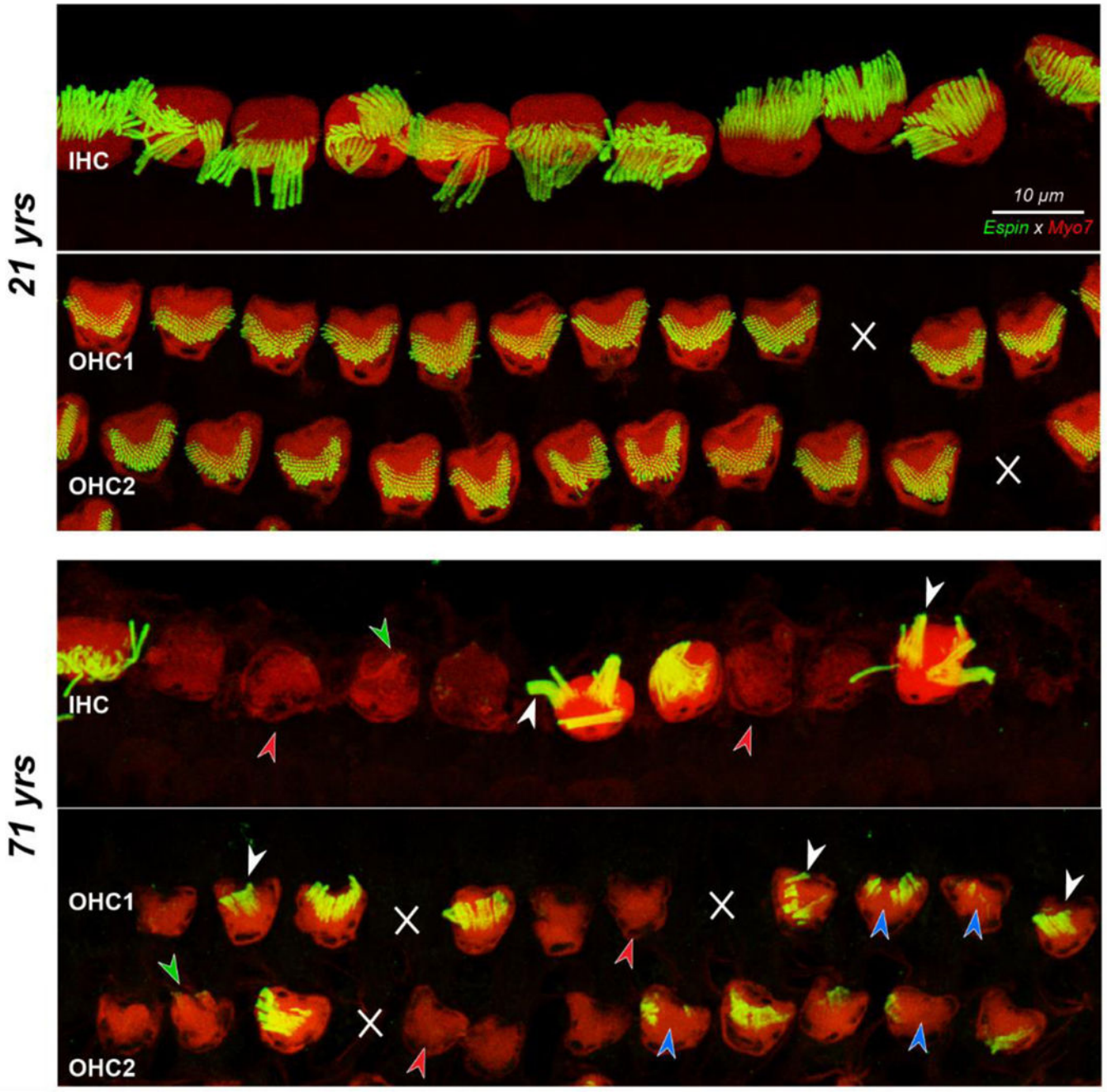

Figure 3:

Confocal images showing IHCs and the first two rows of OHCs with their stereocilia bundles, at the 5.6 kHz region from the 21 yr old and the 71 yr old subject. White X's indicate missing OHCs. Red arrowheads denote hair cells with no stereocilia, blue arrowheads indicate foci of missing stereocilia, and white arrowheads point to fusion bundles. Green arrowheads point to stereocilia bundles visible in the myosin channel that did not stain with espin. Scale bar at the top applies to all panels.

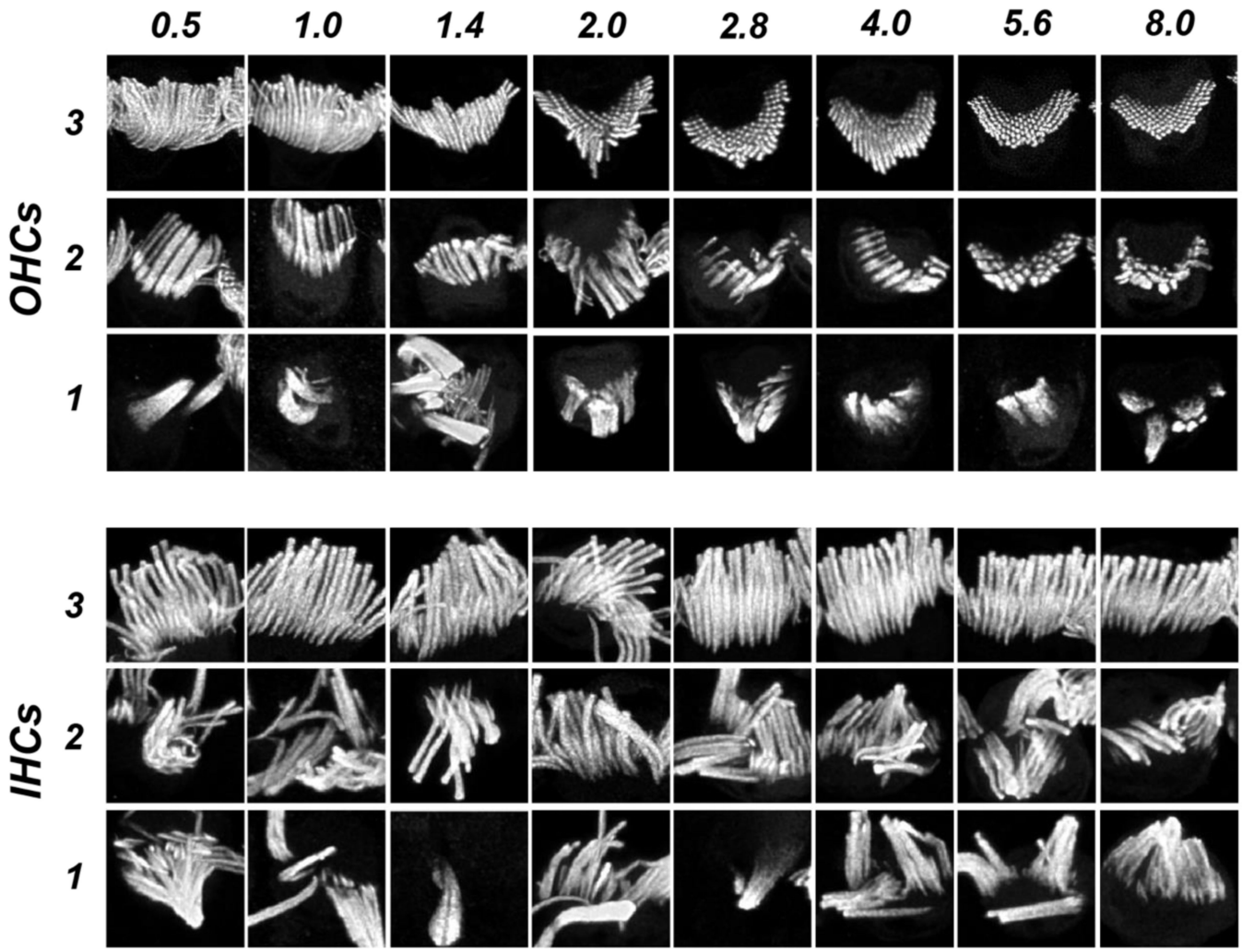

Figure 4:

Image thumbnails from the espin channel of the type used in the blinded semi-quantitative assessment of stereocilia condition, selected as exemplars of OHC and IHC bundles for each of the three non-zero values on the rating scale, at each of the cochlear frequency regions sampled within the audiometric frequency range. Exemplars of “0” ratings are not shown, because there is no signal in the espin channel for those hair cells.

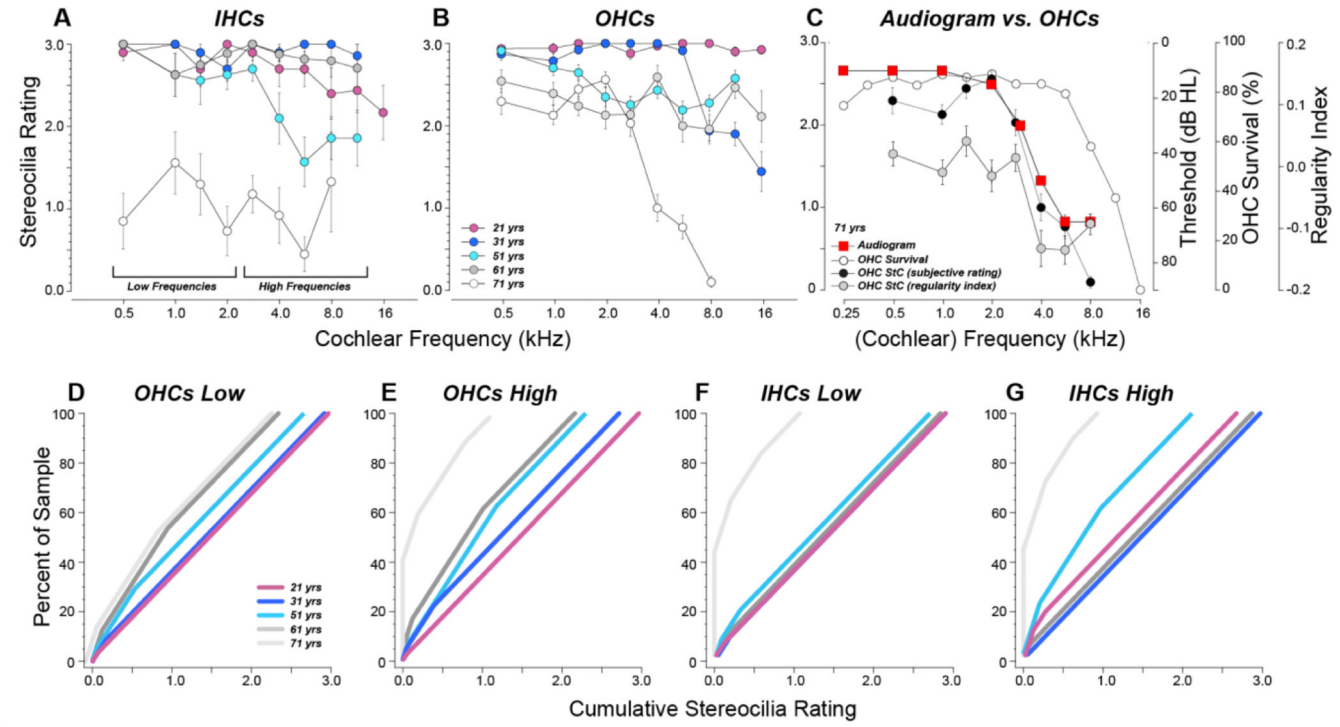

Figure 5:

Stereocilia ratings based on the semi-quantitative rating scale illustrated in Figure 4. **A,B**: Mean data (±SEMs) from each of the five cases. Symbol key in **B** also applies to **A**. **C**: Comparison of stereocilia subjective ratings, stereocilia regularity indexes, and hair cell survival to the audiogram in the oldest ear. OHC survival data are the same as those shown in Figure 1, stereocilia regularity indexes are the same as those in Fig. 8B, and stereocilia subjective ratings are the same as those in **B**. Only data from images with 2 or more surviving hair cells are shown. **D-G**: Cumulative distributions of stereocilia ratings for OHCs (**D,E**) and IHCs (**F,G**) pooled from the four low-frequency cochlear locations (**D,F**) or four high-frequency locations (**E,G**). Plots are generated by arranging the pooled ratings in ascending order and computing the running average while increasing the percentage of the sample included. Symbol key in **D** also applies to **E,F** and **G**.

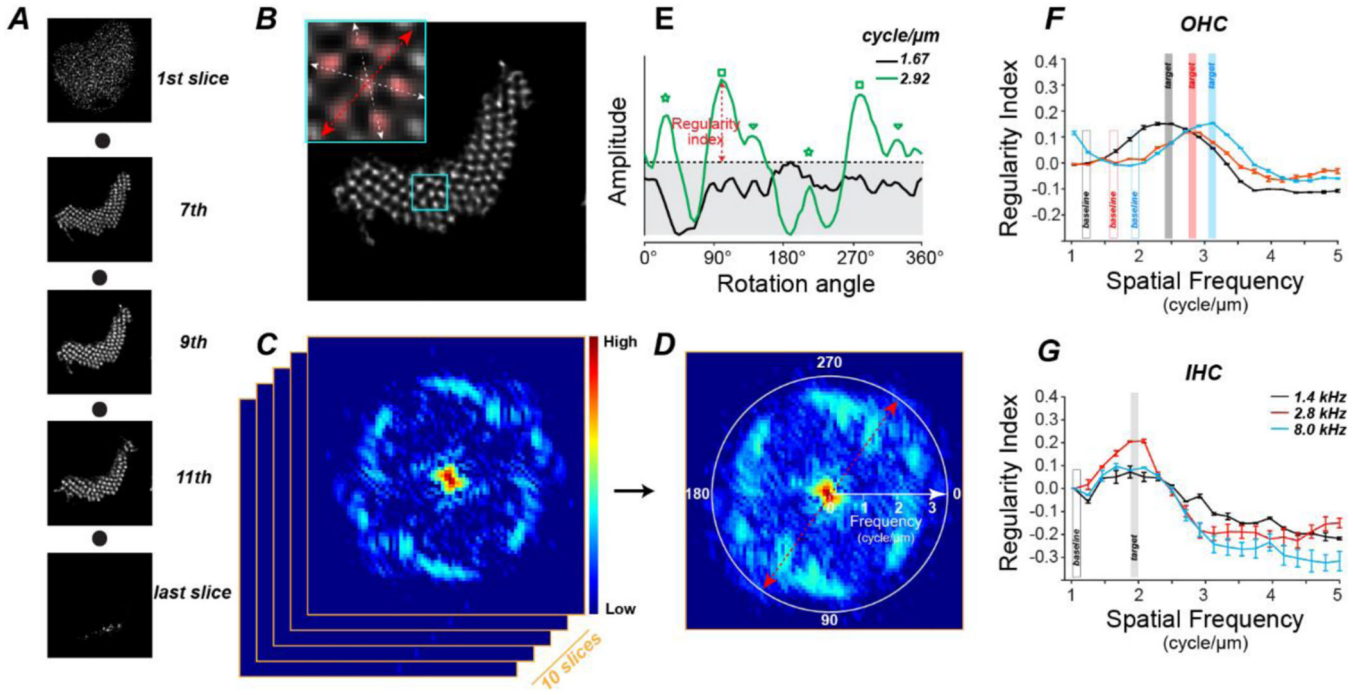

Figure 6:

The algorithm for assessing stereocilia regularity using 2D FFT. **A**: A series of confocal slices from one hair bundle, from the cuticular plate (1st slice) to the stereocilia tips (last slice), of one OHC at 5.6 kHz region. **B**: Detail of the 9th z-slice through the hair bundle shown in **A**. Inset shows the area within the cyan rectangle, highlighting the hexagonal arrangement and the three cardinal axes of the stereocilia. **C**: The 2D FFT spectrum of the slice from **B** with amplitude coded as a heat map. 2D FFT is applied to 10 adjacent confocal slices from the middle of the z-stack. **D**: The maximum projection of the 2D spectra in **C** in polar coordinates, with spectral frequency along the radial axis as shown. Color bar in **C** also applies to **D**. **E**: The amplitude of the maximum-projection spectrum from **D** at two discrete spectral frequencies as a function of rotational angle, smoothed by a moving window average (5 adjacent data points). Regularity index is derived by subtracting the maximum amplitude at the spatial frequency of interest (2.92 cycles/μm in this example) from the maximum amplitude at the baseline frequency (1.67 cycle/μm in this example). Three pairs of green symbols indicate the three pairs of spectral peaks, respectively. **F,G**: Mean regularity indexes (±SEM) from the 21 yr old at 1.4, 2.8, and 8.0 kHz from OHCs (**F**) and IHCs (**G**).Target spatial frequencies for the older ears are defined from the peaks of these curves, as shown., Baseline frequencies are set at the trough below target, as shown.

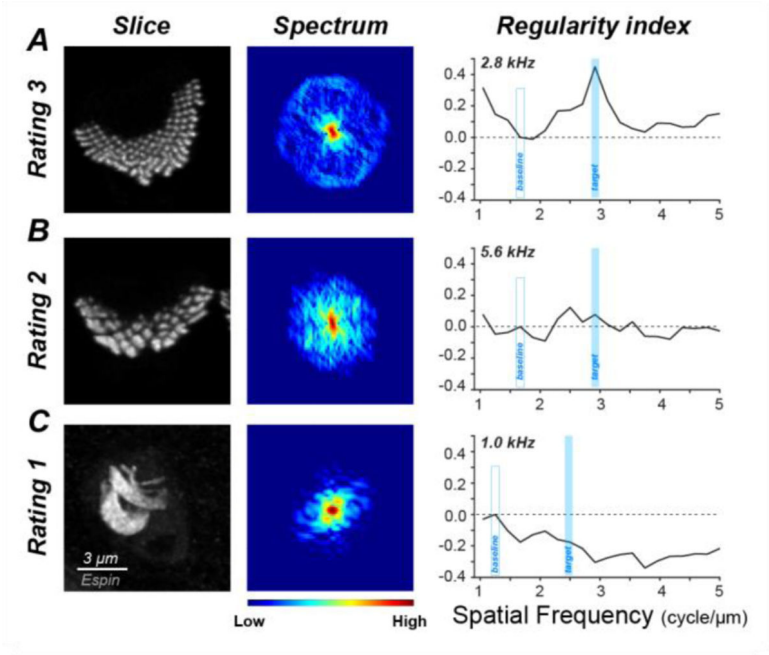

Figure 7:

Confocal projections, 2D spectra and regularity indexes for exemplars of OHC stereocilia bundles for each of the three non-zero values on the rating scale. For each example, the maximum projection of the hair bundle (1st column), the maximum projection of the 10 single-slice spectra (2nd column) and the regularity index as a function of spatial frequency computed from the projection spectrum are shown. The cochlear frequency region is indicated. Scale bar and color bar in **C** applies to all panels.

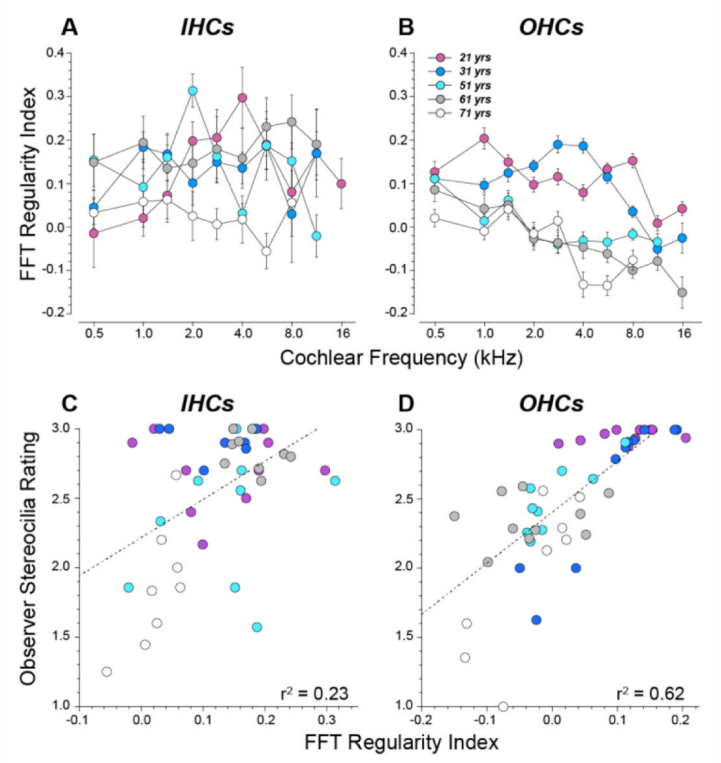

Figure 8:

Regularity indexes derived from the FFT analysis and their correlation with the semi-quantitative ratings from human observers. **A,B**: Mean values (SEMs) of the regularity index (see Figure 6) at each cochlear region in each of the five cases. **C,D**: Comparison of the mean FFT-based stereocilia ratings and the semi-quantitative human-observer ratings for each cochlear region in each case. Hair cells lacking stereocilia bundles were not included in these average values. Best-fit straight lines are shown, along with the r^2 values. Data shown here include only cochlear regions with two or more surviving hair cells. Symbol key in **B** applies to all panels.